Dyes and Pigments 112 (2015) 255–261

Contents lists available at ScienceDirect

Dyes and Pigments

journal homepage: www.elsevier.com/locate/dyepig

Crystallization-induced emission of styrylbenzoxazole derivate with response to proton

Pengchong Xue [a, *], Boqi Yao [a], Jiabao Sun [a], Zhenqi Zhang [a], Kechang Li [b], Baijun Liu [b], Ran Lu [a, *]

[a] State Key Laboratory of Supramolecular Structure and Materials, College of Chemistry, Jilin University, 2519# Jiefang Road, Changchun, PR China
[b] College of Chemistry, Jilin University, Changchun, PR China

ARTICLE INFO

Article history:
Received 17 June 2014
Received in revised form
16 July 2014
Accepted 21 July 2014
Available online 31 July 2014

Keywords:
Enhanced emission
Styrylbenzoxazole
Response
Protonation
Crystal
Excimer

ABSTRACT

A benzoxazole derivative called **BVDA** was synthesized. **BVDA** exhibited an AIE effect although there was H-aggregated dimer in the crystal. According to the spectral results and crystal structure, the presence of excimer and the restriction of intramolecular rotation are responsible for the AIE phenomenon. Moreover, **BVDA** could respond to proton in solution and to volatile acid vapours in film. **BVDA** exhibited three colours because its binding sites to proton have different basicities. These binding sites can then be protonated in turn. These results indicate that AIE fluorophores with H-aggregated dimer is possible. Furthermore, these fluorophores can exhibit stimuli-responsive characteristics through the introduction of functional moieties.

1. Introduction

Highly efficient emission of organic molecules in solid state is essential in optoelectronic devices, such as organic light-emitting diodes (OLEDs), organic light-emitting field-effect transistors, organic solid-state lasers, and organic fluorescent sensors [1]. However, achieving strong emission for organic molecules in solid or crystal state is extremely difficult. One cause of the quenching process is mechanistically associated with "aggregation-caused quenching" because of the quick de-excitation of excited fluorophores through internal conversion, intersystem crossing, intramolecular charge transfer, intermolecular electron transfer, excimer or exciplex formation, or isomerization. In fact, there are some reports to disclose organic fluorophores with strong emission in solid [2]. More importantly, the group of Tang discovered a silole derivative in 2001, exhibiting dramatically enhanced emission in solid state, and named this phenomenon aggregation-induced emission (AIE) or aggregation-induced enhanced emission [3]. Many AIE molecules have been developed and applied in OLEDs, piezochromism, fluorescent sensors and probes, bioimaging, and fluorescent switch [4]. Generally, AIE molecules have twisted configurations and freely rotated single bonds, such as silole, tetraphenylethene, 9,10-distryrylanthracene, and cyano-diphenylethene derivatives [5]. In solid or crystal state, intramolecular rotation is suppressed, and the twisted configuration leads to loose stacking, which promotes strong emission relative to the solutions. The formation of J-aggregates can also activate radiative transition and cause fluorophores to exhibit AIE properties [6]. However, fluorescent H-aggregates that exhibit AIE behaviour are rarely reported, although some emissive dyes in H-aggregate have been observed [7].

As we know, **BVDA** is one fluorescent molecule and have been applied in fluorescence probe for cell, solvent polarity, and PH [8]. In the present study, we found that **BVDA** exhibited weak emission in solutions but emitted strong fluorescence in crystal state. Spectral result and single-crystal structure suggest that the presence of anti-parallel H-aggregated dimer should be responsible for emission enhancement. Moreover, **BVDA** exhibited dual-mode response to proton and to volatile acid vapour in the solution and crystal state, respectively.

2. Experimental section

2.1. General information

All the raw materials were used without further purification. All the solvents as analytical reagent were purchased from Beijing Chemical Works (Beijing, China), and were used without further

* Corresponding authors.
E-mail addresses: xuepengchong@jlu.edu.cn (P. Xue), luran@mail.jlu.edu.cn (R. Lu).

http://dx.doi.org/10.1016/j.dyepig.2014.07.026
0143-7208/

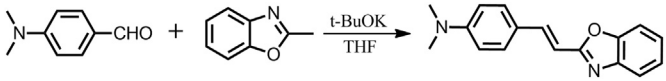

Scheme 1. Synthesis route of **BDVA**.

purification. Water used throughout all experiments was purified with the Millipore system. The UV–vis absorption spectra were obtained using a Mapada UV-1800pc spectrophotometer. Photoluminescence measurements were taken on a Cary Eclipse Fluorescence Spectrophotometer. The fluorescence quantum yields of **BVDA** in solvents were measured by comparing to a standard (9,10-diphenyl anthracene in benzene, $\Phi_F = 0.85$). The excitation wavelength was 375 nm. The absolute fluorescence quantum yield of **BVDA** crystal was measured on an Edinburgh FLS920 steady state fluorimeter using an integrating sphere. Fluorescence decay experiment was measured on an Edinburgh FLS920 steady state fluorimeter equipped with an nF900 ns flash lamp. Mass spectra were obtained with AXIMA CFR MALDI-TOF (Compact) mass spectrometers. C, H, and N elemental analyses were performed with a Perkin–Elmer 240C elemental analyzer. Single crystal was obtained in the mixture of CH_2Cl_2 and n-hexane by slow solvent diffusion method. The molecular configuration in crystal was used to obtain frontier orbitals of **BVDA** by density functional theory (DFT) calculations at B3LYP/6-31G level with the Gaussian 09W program package [9].

Single crystal of **BVDA** was selected for X-ray diffraction analysis on in a Rigaku RAXIS-RAPID diffractometer using graphite-monochromated Mo-Kα radiation (λ = 0.71073 Å). The crystal was kept at room temperature during data collection. The structures were solved by the direct methods and refined on F2 by full-matrix least-square using the SHELXTL-97 program [10]. The C, N, O and H atoms were easily placed from the subsequent Fourier-difference maps and refined anisotropically. CCDC 994905 contains the supplementary crystallographic data for this paper.

2.2. Synthesis of BVDA

(E)-4-(2-(benzo[d]oxazol-2-yl)vinyl)-*N*,*N*-dimethylaniline (**BVDA**)

t-BuOK (2.2 g, 19.6 mmol) was added into dry THF (20 mL) and stirred for 10 min at 0 °C. 2-methylbenzoxazole (0.3 mL, 10.8 mmol) was dropwise added into above suspension and stirred for 10 min at 0 °C. Then, a THF solution of 4-(dimethylamino)benzaldehyde (1.47 g, 9.8 mmol) was dropped slowly into the above solution at 0 °C. After stirred for 2 h, the mixture was poured into water (200 mL) and yellow solid was collected by filtration. The crude product was purified by a silica gel column using CH_2Cl_2 as the eluent. Yellow platy crystal was obtained in a yield of 81% (2.1 g). mp: 181–182 °C. FT-IR: 3091, 3064, 3054, 3010, 2982, 2982, 2894, 2816, 1635, 1603, 1555, 1537, 1455, 808, and 746 cm^{-1}. Element analysis (%): calculated for $C_{17}H_{16}N_2O$: C, 77.25; H, 6.10; N, 10.60; Found: C, 77.20; H, 6.30; N, 10.68. ^{1}H NMR (400 MHz, $CDCl_3$) δ 7.76 (*t*, *J* = 16.2 Hz, 1H), 7.72–7.67 (m, 1H), 7.56–7.49 (m, 3H), 7.36–7.30 (m, 2H), 6.88 (*d*, *J* = 16.2 Hz, 1H), 6.76 (*d*, *J* = 8.6 Hz, 2H), 3.06 (*s*, 6H). MALDI-TOF MS: *m*/*z*: calcd for $C_{17}H_{16}N_2O$: 264.1; found: 265.1 $(M + H)^+$.

3. Results and discussion

BVDA as yellow platy crystal was synthesized through a one-step reaction (Scheme 1) with a yield of 81%. **BVDA** easily dissolved in CH_2Cl_2, $CHCl_3$, benzene, toluene, THF, DMF, and so on, but exhibited low solubility in cyclohexane and hexane. Moreover, **BVDA** solutions have different absorption and emission spectra (Table S1). The maximal absorption peak was observed at 378 nm in cyclohexane, a red-shifted peak (389 nm) for toluene solution appeared, and the DMF solution possessed an absorption band (λ_{ab} = 394 nm) with the lowest energy (Fig. 1a). A structured emission band with a maximum absorption peak at 434 nm and a shoulder peak at 456 nm was observed in cyclohexane. With an increase in solvent polarity, the emission wavelength of the solutions shifted to the low energy region, and the emission bands became structureless. A red shift in the emission wavelength indicates the excited state of **BVDA** with stronger polarity than that in ground state [11], and absorption and emission bands in different solvents could be ascribed to intramolecular charge transfer (ICT) transition. The quantum-chemical calculation confirmed the ICT transition. Fig. 1c shows that the dimethylaniline group has a larger density than benzoxazole in the highest occupied frontier molecular orbital (HOMO). As the electron density of the lowest unoccupied molecular orbital (LUMO) of the dimethylaniline unit decreases, the benzoxazole and vinyl moieties achieve large

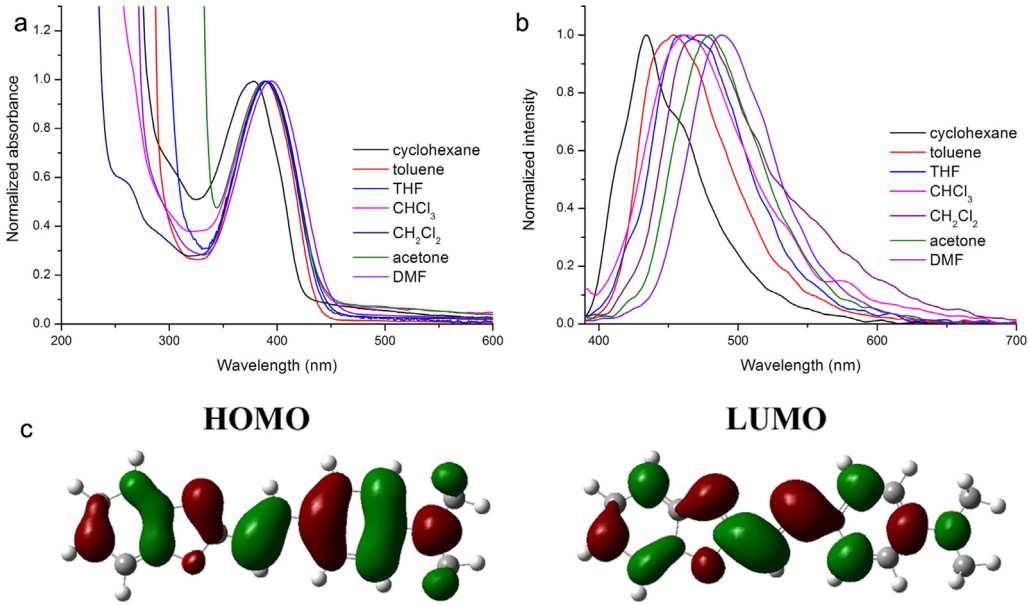

Fig. 1. (a) Absorption and (b) fluorescence spectra of **BVDA** in different solvents, and (c) frontier orbitals of **BVDA**.

electron density. The stimulated absorption spectrum of **BVDA** exhibited a strong absorption band at ca. 375 nm, which attributed to the HOMO → LUMO transition (Table S2) [12]. Light excitation clearly induced electron transfer from the donor unit to the acceptor. This result further proves that absorption in the long wavelength region and emission are ascribed to ICT transition.

Becasue **BVDA** consists of two binding sites to proton, the response of **BVDA** to proton was expected. When TFA was gradually added to the $CHCl_3$ solution of **BVDA**, the solution turned orange. The further addition of TFA bleached the orange solution (Fig. 2c). The change in absorption spectra also supports this phenomenon. Fig. 2a shows that the THF solution possesses one absorption peak at 390 nm and that the absorption edge ranges from 400 nm to 450 nm, which causes the solution to take on yellowish. When TFA was added, this absorption peak gradually decreased, and a new peak at 475 nm emerged and increased along with TFA concentration (Fig. S3). After the addition of 36 equiv TFA, the absorption peak at 475 nm reached the maximum, at which point the solution turned orange. Further addition of TFA induced a decrease of the absorption peak at 475 nm. With 500 equiv TFA, the absorbance in the visible region was so weak that the solution was almost colourless.

The ^{1}H NMR spectra before and after the addition of TFA were measured and compared to verify the cause of the colour transformation (Fig. 3). We found that the addition of TFA caused the signals to display a low field shift for all protons, which is indicative of binding to proton. Considering that the N atom of benzoxazole has stronger basicity than dimethylaniline moiety, proton first bound to the benzoxazole group to form **BVDAH**, which enhanced the electron withdrawing ability of benzoxazole moiety and caused the red shift in absorption spectrum [13]. When dimethylaniline started protonation, the sp2 hybridized N of the dimetylamino unit transformed into sp3 hybridized one and **BVDA2H** formed, which resulted in the disappearance of ICT absorption and a hypsochromic absorption band. Quantum chemical calculation supports our hypothesis (Fig. S4, Fig S5 and Table S2). The absorption peak of **BVDA** was calculated at 375 nm, and that of **BVDAH** appeared at 432 nm. After bound two protons, the absorption band located 400 and 380 nm.

The fluorescence of **BVDA** in $CHCl_3$ solution can also respond to proton. The emission band around 460 nm decreased upon the addition of TFA, and one new emission band emerged with a maximum absorption peak of 525 nm (Fig. 2b). The emission colour changed from blue to green. The emission band at 525 nm reached its maximum upon the addition of 6 equiv TFA. Further addition of TFA led to a continuous decrease of this emission band. With excess TFA, the fluorescence colour shifted to blue again, and the emission intensity weakened.

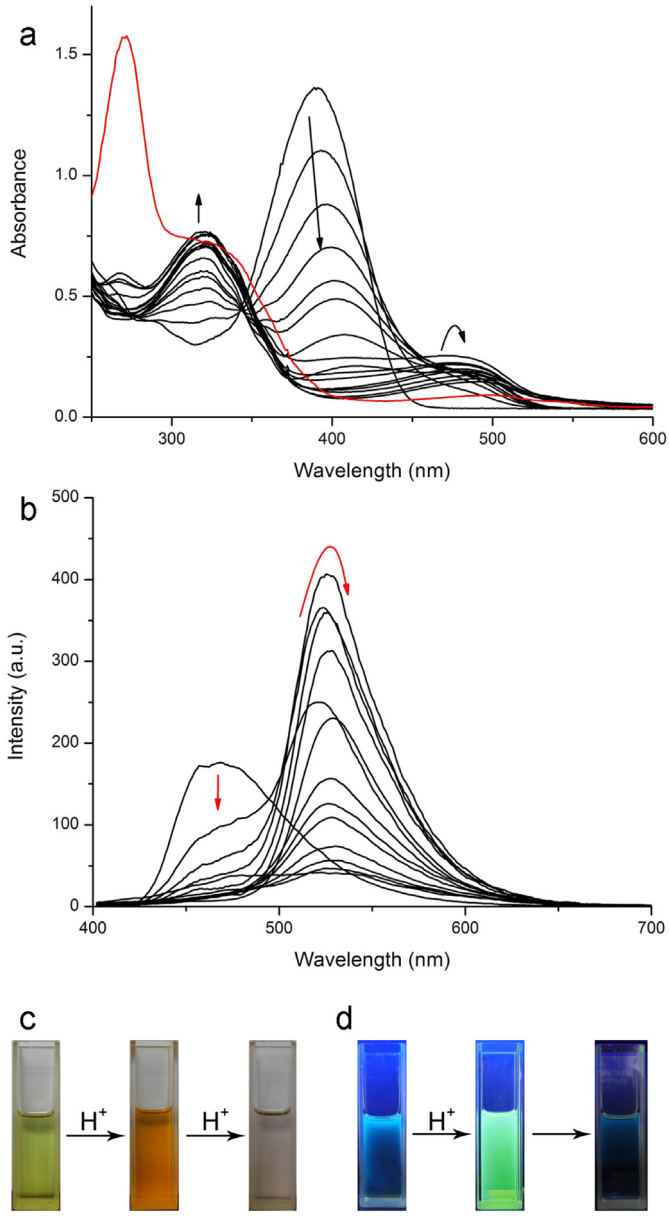

Fig. 2. (a) Absorption and (b) emission spectral change in **BVDA** in $CHCl_3$ (10^{-4} M) from 0 equiv to 500 equiv. Excitation wavelength is 375 nm. The red line is the absorption spectrum with 500 equiv TFA. Photos of **BVDA** solution under (c) natural light and (c) 365 nm light.

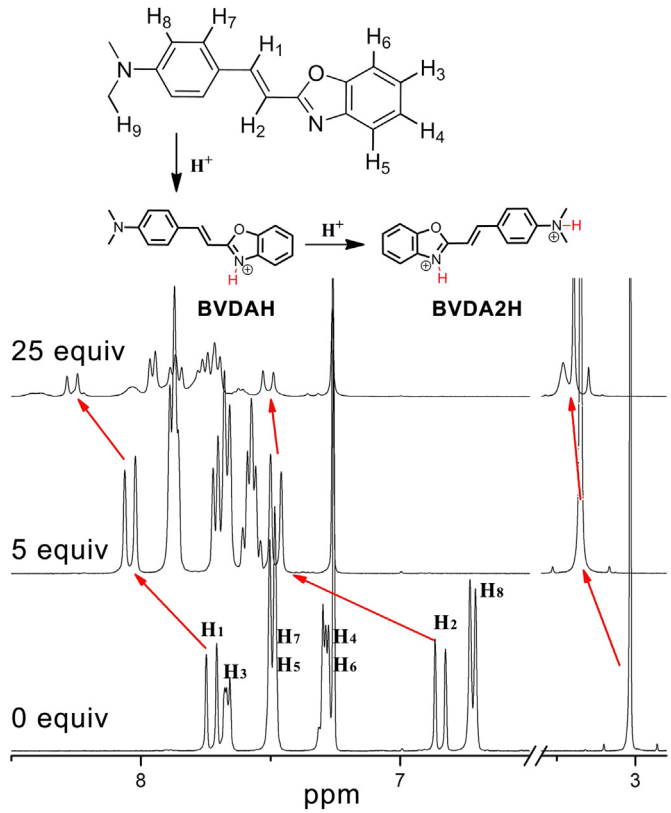

Fig. 3. ^{1}H NMR spectra of **BVDA** in $CDCl_3$ upon addition of TFA.

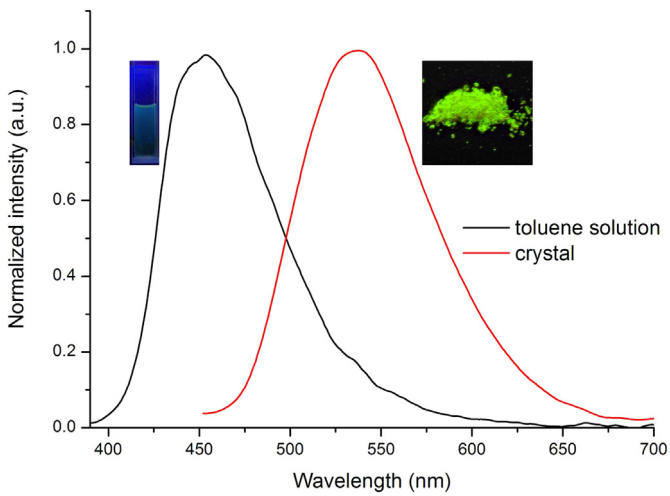

Fig. 4. Fluorescence spectra of **BVDA** in toluene and crystal state. Insets are photos under 365 nm light.

The **BVDA** solutions were found to emit weak fluorescence, but the yellow as-synthesized platy crystal of **BVDA** exhibited extremely strong yellow green fluorescence under 365 nm light (Fig. 4). **BVDA** in cyclohexane exhibited a fluorescence quantum yield Φ of 0.034, whereas **BVDA** in toluene exhibited a low Φ of 0.009 (Table S1). On the other hand, **BVDA** crystal with yellow green emission (λ_{em} = 535 nm, Fig. 4) had a Φ value of 0.67. This result suggests that **BVDA** is AIE active. [14] The mixed solvent system comprising THF and water was selected to confirm the AIE-active **BVDA** [15]. Fig. 5 shows the absorption and emission spectra of **BVDA** in mixed solvents. When water content was less than 70%, the red-shifted absorption spectra emerged as a result of an increase in solvent polarity. When water content increased to 80%, absorbance started to decrease and undergo blue shifting, which indicated that the molecule started to form aggregates [16]. However, emission intensity was independent of solvent even water content reached 90%. Moreover, it was found that the yellow plate-like microcrystal with strong emission formed when the suspension contained 90% water was aged 10 h. This result indicates that the restriction of intramolecular rotation (RIR) and the ordered arrangement are responsible for its strong yellow green fluorescence. So, **BVDA** should be a crystallization-induced emission fluorophore [17].

The single-crystal structure of **BVDA** was obtained to understand the mechanism of the AIE phenomenon and establish structure–property relationships. The single crystal of **BVDA** belongs to orthorhombic space group P bca with eight molecules per unit cell ($Z = 8$, see Table S3 for the crystallographic data). In crystal, two molecules first formed anti-parallel dimer with a distance of 3.44 Å (Fig. 6), which implies strong π–π interaction [18]. Then, many dimers arranged into a herringbone structure (Fig. S6). In addition, one **BVDA** molecule comprises four weak CH–π and

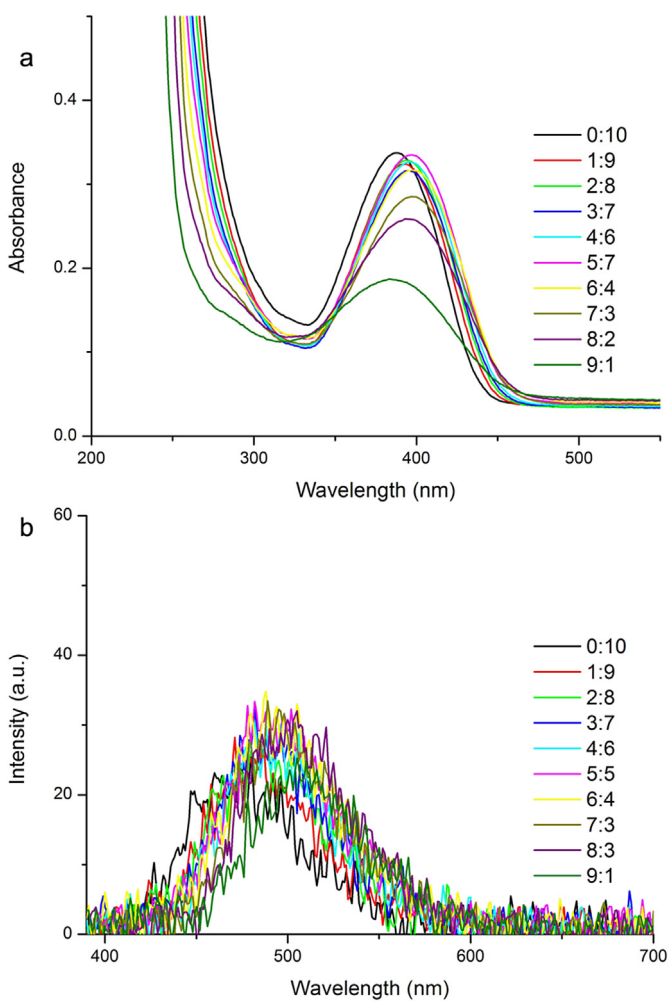

Fig. 5. (a) UV–vis absorption and (b) fluorescence emission spectra (λ_{ex} = 375 nm) of **BVDA** (1.0×10^{-5} M) in THF–water with different amounts of water (% volume).

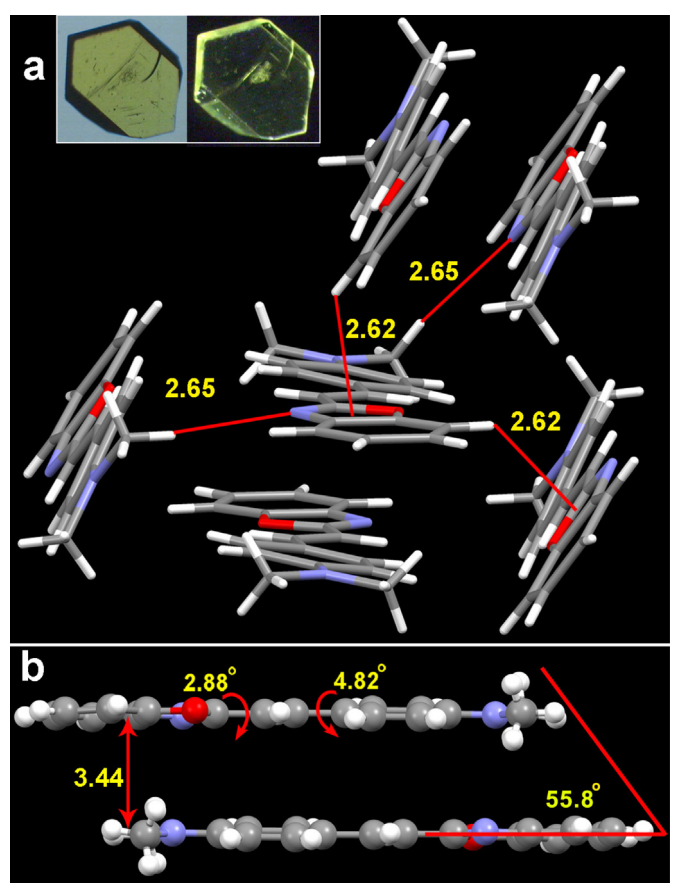

Fig. 6. Crystal packing of **BVDA** with different intermolecular interactions: (a) CH–π and CH–N hydrogen bonds; (b) π–π interaction for dimer. Inset is single crystal under natural and 365 nm UV light.

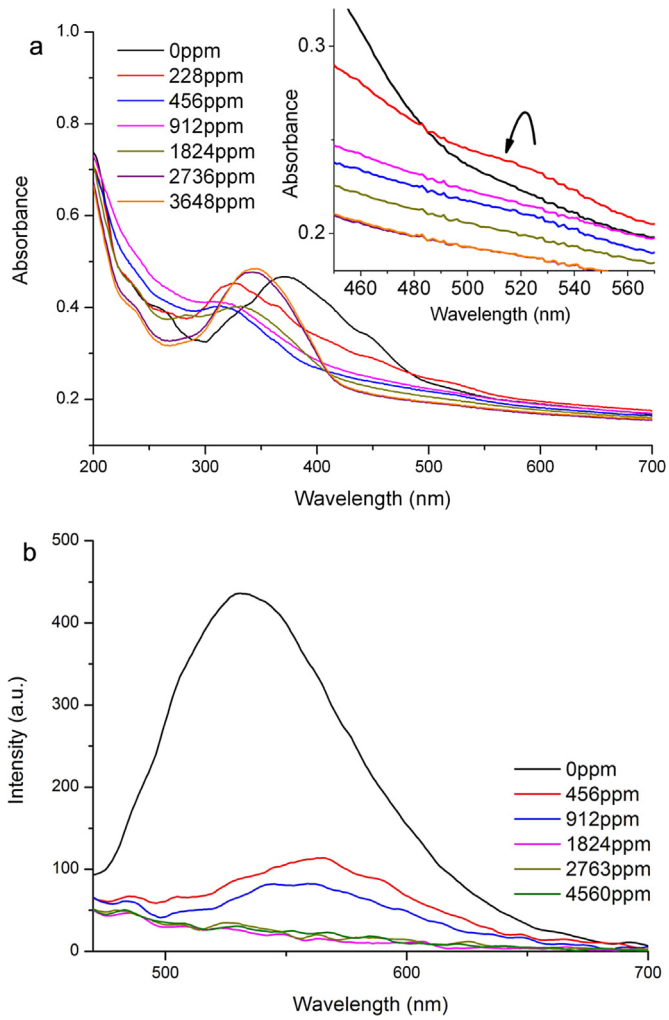

Fig. 7. Absorption (a) and fluorescence (b) spectra of **BVDA** film upon exposure to TFA. $\lambda_{ex} = 375$ nm.

CH—N hydrogen bonds with adjacent four molecules. This structure suppresses the free rotation of a single bond. The dihedral angles are small, thus suggesting good conjugation in crystal. The optimal structure of TD/DFT-B3LYP/6-31G reveals that molecule in vacuum adopts a planar conformation (Fig. S5). Thus, planarization does not cause the strong emission of **BVDA** in crystal state, and *cis-trans* isomerization and intramolecular free rotation of single bond may be reason of weak emission for **BVDA** in solutions [19]. Fig. S7 indicates that the crystal exhibits a blue-shifted absorption band relative to that of the solution. Moreover, a large slip angle of 55.8° between two molecules in dimer was observed. These results suggest that the dimer is a face-to-face H-aggregate [20]. Considering broad emissive band and large Stokes shift, the yellow-green emission of BVDA crystal is originated from the excimer induced by light irradiation [21]. The result of time-resolved fluorescence spectra also supports our hypothesis. In toluene, the fluorescence lifetime (τ) is 0.59 ns (Fig. S8), and a radiative rate of 0.015 ns^{-1} can be extracted. On the other hand, yellow crystal has a very long τ of 63.2 ns, and a relative slow radiative rate (0.011 ns^{-1}). Slow deactivation of excited state in crystal suggests H-aggregate, and long lifetime confirms the red-shifted emission of crystal indeed originates from excimer [22]. Thus, the large Φ of yellow crystal should be attributed to RIR and to the presence of excimer.

The above results indicate that **BVDA** solutions can respond to proton in terms of colour and fluorescence. The response of the **BVDA** crystal with strong emission to the volatile acid was expected [23]. The colour of the crystal film was strongly dependent on the concentration of TFA vapour. The crystal film was yellow in the absence of TFA and turned red when the TFA concentration was 228 ppm. The disappearance of the absorption peak at 370 nm and the emergence of a new absorption band at around 510 nm also explained the red colour of the film (Fig. 7a). Further increasing TFA concentration weakened the absorbance in the visible region. When TFA concentration reached 2736 ppm, the red film became colourless. The change in the fluorescence spectra was similar to that in the absorption spectra (Fig. 7b). The yellow green fluorescence turned to red and gradually decreased in emission intensity. Emission was completely quenched upon exposure of the film to TFA with high concentration. We also found that the colourless film turned red and not yellow after exposing to air. This result suggests that proton escaped from N of the dimethylaniline unit and that benzoxazole moiety continued to undergo protonation. A red film could rapidly revert to its yellow colour upon exposure to NH_3 vapour (Fig. S9). Thus, our emissive crystal film reversibly responds to volatile acid vapour in three colours. The test paper, prepared by soaking filter paper in $CHCl_3$ solution of **BVDA** and then air-drying, also possessed the similar responsive behaviour to that of the crystal film (Fig. 8). Yellow test paper changed into red one in TFA vapour with low concentration, and turned into colourless one with high concentration TFA vapour. Red and colourless papers could restore original yellow by exposing their to NH_3 vapour, so such test paper was used repeatedly. Therefore, our crystal film and test film have superiority over common PH indicators because they can be used to detect acid vapour and be able to recycle.

4. Conclusions

In summary, we discovered that a benzoxazole derivative called **BVDA** exhibited an AIE effect although H-aggregated dimer in the crystal existed. According to the spectral results and quantum-chemical calculation, the presence of excimer and RIR are responsible for the AIE phenomenon. Moreover, **BVDA** can respond to proton in solution and to volatile acid vapour in film. **BVDA** exhibits three colours because its binding sites to proton have different basicities. These results indicate that fluorophores with H-

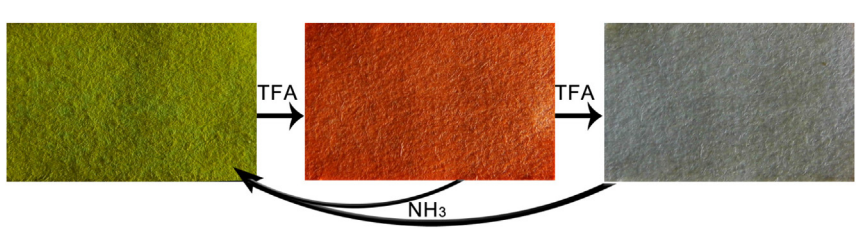

Fig. 8. Photos of filter paper consisting of **BDVA** in response to TFA vapour.

aggregated dimer is possible to exhibit AIE activity and have unique properties.

Acknowledgements

This work was financially supported by the National Natural Science Foundation of China (21103067, and 21374041), the Youth Science Foundation of Jilin Province (20130522134JH), the Science and Technology Development Plan of Jilin Province, China (20130521003JH), the Open Project of the State Key Laboratory of Supramolecular Structure and Materials (SKLSSM201407), the Open Project of State Laboratory of Theoretical and Computational Chemistry (K2013-02).

Appendix A. Supplementary data

Supplementary data related to this article can be found at http://dx.doi.org/10.1016/j.dyepig.2014.07.026.

References

[1] a) Minaev B, Baryshnikov G, Agren H. Principles of phosphorescent organic light emitting devices. Phys Chem Chem Phys 2014;16:1719–58;
b) Wang C, Dong H, Hu W, Liu Y, Zhu D. Semiconducting π-conjugated systems in field-effect transistors: a material odyssey of organic electronics. Chem Rev 2012;112:2208–67;
c) Basabe-Desmonts L, Reinhoudt DN, Crego-Calama M. Design of fluorescent materials for chemical sensing. Chem Soc Rev 2007;36:993–1017;
d) Carter KP, Young AM, Palmer AE. Fluorescent sensors for measuring metal ions in living systems. Chem Rev 2014;114:4564–601.

[2] a) Oelkrug D, Tompert A, Gierschner J, Egelhaaf H, Hanack M, Hohloch M, et al. J Phys Chem B 1998;102:1902–7;
b) Dykstra TE, Hennebicq E, Beljonne D, Gierschner J, Claudio G, Bittner ER, et al. Conformational disorder and ultrafast exciton relaxation in PPV-family conjugated polymers. J Phys Chem B 2009;113:656–67;
c) Beljonne D, Curutchet C, Scholes GD, Silbey RJ. Beyond förster resonance energy transfer in biological and nanoscale systems. J Phys Chem B 2009;113:6583–99;
d) Yoon S, Chung JW, Gierschner J, Kim K, Choi M, Kim D, et al. Multistimuli two-color luminescence switching via different slip-stacking of highly fluorescent molecular sheets. J Am Chem Soc 2010;132:13675–83.

[3] a) Luo J, Xie Z, Lam JWY, Cheng L, Chen H, Qiu C, et al. Aggregation-induced emission of 1-methyl-1,2,3,4,5-pentaphenylsilole. Chem Commun 2001:1740–1;
b) Hong Y, Lam JWY, Tang BZ. Aggregation-induced emission. Chem Soc Rev 2011;40:5361–88.

[4] a) Song Z, Hong Y, Kwok RTK, La JWY, Liu B, Tang BZ. A dual-mode fluorescence "turn-on" biosensor based on an aggregation-induced emission luminogen. J Mater Chem B 2014;2:1717–23;
b) Chi Z, Zhang X, Xu B, Zhou X, Ma C, Zhang Y, et al. Recent advances in organic mechanofluorochromic materials. Chem Soc Rev 2012;41:3878–96;
c) Huang J, Tang R, Zhang T, Li Q, Yu G, Xie S, et al. A new approach to prepare efficient blue AIE emitters for undoped OLEDs. Chem Eur J 2014;20:5317–26;
d) Li X, Ma K, Zhu S, Yao S, Liu Z, Xu B, et al. Fluorescence turn-on detection of DNA and label-free fluorescence nuclease assay based on the aggregation-induced emission of silole. Anal Chem 2014;86:298–303;
e) Liao Y, Li K, Wu M, Wu T, Yu X. A selenium-contained aggregation-induced "turn-on" fluorescent probe for hydrogen peroxide. Org Biomol Chem 2014;12:3004–8;
f) Wang Y, Liu W, Bu L, Li J, Zheng M, Zhang D, et al. Reversible piezochromic luminescence of 9,10-bis[(N-alkylcarbazol-3-yl)vinyl]anthracenes and the dependence on N-alkyl chain length. J Mater Chem C 2013;1:856–62;
g) Zheng M, Sun M, Li Y, Wang J, Bu L, Xue S, et al. Piezofluorochromic properties of AIE-active 9,10-bis(N-alkylpheno-thiazin-3-yl-vinyl-2)anthracenes with different length of alkyl chains. Dyes Pigment 2014;102:29–34.

[5] a) Zhang H, Guo E, Zhang Y, Ren P, Yang W. Donor-acceptor-substituted anthracene-centered cruciforms: synthesis, enhanced two-photon absorptions, and spatially separated frontier molecular orbitals. Chem Mater 2009;21:5125–35;
b) Xie Z, Yang B, Cheng G, Liu L, He F, Shen F, et al. Supramolecular interactions induced fluorescence in crystal: anomalous emission of 2,5-diphenyl-1,4-distyrylbenzene with all cis double nonds. Chem Mater 2005;17:1287–9;
c) Li Y, Li F, Zhang H, Xie Z, Xie W, Xu H, et al. Tight intermolecular packing through supramolecular interactions in crystals of cyano substituted oligo(para-phenylene vinylene): a key factor for aggregation-induced emission. Chem Commun 2007:231–3;
d) Shen X, Wang Y, Zhao E, Yuan W, Liu Y, Lu P, et al. Effects of substitution with donor–acceptor groups on the properties of tetraphenylethene trimer: aggregation-induced emission, solvatochromism, and mechanochromism. J Phys Chem C 2013;117:7334–47.

[6] a) Yoon S, Kim JH, Chung JW, Park SY. Exploring the minimal structure of a wholly aromatic organogelator: simply adding two β-cyano groups to distyrylbenzene. J Mater Chem 2011;21:18971–3;
b) Xu Y, Xue P, Xu D, Zhang X, Liu X, Zhou H, et al. Multicolor fluorescent switches in gel systems controlled by alkoxyl chain and solvent. Org Biomol Chem 2010;8:4289–96;
c) Xu D, Liu X, Lu R, Xue P, Zhang X, Zhou H, et al. New dendritic gelator bearing carbazole in each branching unit: selected response to fluoride ion in gel phase. Org Biomol Chem 2011;9:1523–8;
d) Chowdhury A, Wachsmann-Hogiu S, Bangal PR, Raheem I, Peteanu LA. Characterization of chiral H and J aggregates of cyanine dyes formed by DNA templating using stark and fluorescence spectroscopies. J Phys Chem B 2001;105:12196–201;
e) An B, Kwon S, Jung S, Park SY. Enhanced emission and its switching in fluorescent organic nanoparticles. J Am Chem Soc 2002;124:14410–5;
f) Wang Y, Liu T, Bu L, Li J, Yang C, Li X, et al. Aqueous nanoaggregation-enhanced one- and two-photon fluorescence, crystalline J-aggregation-induced red shift, and amplified spontaneous emission of 9,10-bis(p-dimethylaminostyryl)anthracene. J Phys Chem C 2012;116:15576–83.

[7] a) Rösch U, Yao S, Wortmann R, Würthner F. Fluorescent H-aggregates of merocyanine Dyes. Angew Chem Int Ed 2006;45:7026–30;
b) Gierschner J, Park SY. Luminescent distyrylbenzenes: tailoring molecular structure and crystalline morphology. J Mater Chem C 2013;1:5818–32;
c) Gierschner J, Ler L, Milin-Madina B, Oelkrug D, Egelhaaf H. highly emissive H-aggregates or aggregation-induced emission quenching? the photophysics of all-trans para-distyrylbenzene. J Phys Chem Lett 2013;4:2686–97.

[8] a) Mishra A, Chaterjee S, Krishnamoorthy G. Intramolecular charge transfer emission of trans-2-[4′-(dimethylamino)styryl]benzimidazole: effect of solvent and pH. J Photochem Photobiol A Chem 2013;260:50–8;
b) Fayed TA. Intramolecular charge transfer and photoisomerization of 2-(p-dimethylaminostyryl) benzoxazole: a new fluorescent probe. J Photochem Photobiol A Chem 1999;121:17–25;
c) Fayed TA, Ali SS. Protonation dependent photoinduced intramolecular charge transfer in 2–(p–dimethylaminostyryl) benzazoles. Spectr Lett 2003;36:375–86.

[9] Frisch MJ, Trucks GW, Schlegel HB, Scuseria GE, Robb MA, Cheeseman JR, Scalmani G, et al. Gaussian 09, revision A02. Wallingford CT: Gaussian, Inc; 2009.

[10] Sheldrick GM. SHELXL-97 program crystal structure refinement. Germany: University of Göttingen; 1997.

[11] a) Loiseau F, Campagna S, Hameurlaine A, Dehaen W. Dendrimers made of porphyrin cores and carbazole chromophores as peripheral units. Absorption spectra, luminescence properties, and oxidation behavior. J Am Chem Soc 2005;127:11352–63;
b) Liu X, Xu D, Lu R, Li B, Qian C, Xue P, et al. Luminescent organic 1D nanomaterials based on bis(β-diketone)carbazole derivatives. Chem Eur J 2011;17:1660–9.

[12] a) Nandy R, Sankararaman S. Donor-acceptor substituted phenylethynyltriphenylenes–excited state intramolecular charge transfer, solvatochromic absorption and fluorescence emission. Beilstein J Org Chem 2010;6:992–1001;
b) Jia J, Zhang Y, Xue P, Zhang P, Zhao X, Liu B, et al. Synthesis of dendritic triphenylamine derivatives for dye-sensitized solar cells. Dyes Pigments 2013;96:407–13.

[13] Xue P, Chen P, Jia J, Xu Q, Sun J, Yao B, et al. A triphenylamine-based benzoxazole derivative as a high-contrast piezofluorochromic material induced by protonation. Chem Commun 2014;50:2569–71.

[14] a) Zhang G, Aldred MP, Gong W, Li C, Zhu M. Utilising tetraphenylethene as a dual activator for intramolecular charge transfer and aggregation induced emission. Chem Commun 2012;48:7711–3;
b) Zhao X, Xue P, Wang K, Chen P, Zhang P, Lu R. Aggregation-induced emission of triphenylamine substituted cyanostyrene derivatives. New J Chem 2014;38:1045–51;
c) Geng J, Zhu Z, Qin W, Ma L, Hu Y, Gurzadyan GG, et al. Near-infrared fluorescence amplified organic nanoparticles with aggregation-induced emission characteristics for in vivo imaging. Nanoscale 2014;6:939–45;
d) Gao B, Wang H, Hao Y, Fu L, Fang H, Jiang Y, et al. Time-resolved fluorescence study of aggregation-induced emission enhancement by restriction of intramolecular charge transfer state. J Phys Chem B 2010;114:128–34.

[15] Liu W, Wang Y, Sun M, Zhang D, Zheng M, Yang W. Alkoxy-position effects on piezofluorochromism and aggregation-induced emission of 9,10-bis(alkoxystyryl)anthracenes. Chem Commun 2013;49:6042–4.

[16] a) Huang J, Sun N, Chen P, Tang R, Li Q, Ma D, et al. Largely blue-shifted emission through minor structural modifications: molecular design, synthesis, aggregation-induced emission and deep-blue OLED application. Chem Commun 2014;50:2136–8;
b) Ananthakrishnan SJ, Varathan E, Ravindran E, Somanathan N, Subramanian V, Mandal AB, et al. A solution processable fluorene–fluorenone oligomer with aggregation induced emission enhancement. Chem Commun 2013;49:10742–4;
c) Liu J, Meng Q, Zhang X, Lu X, He P, Jiang L, et al. Aggregation-induced emission enhancement based on 11,11,12,12-tetracyano-9,10-anthraquinodimethane. Chem Commun 2013;49:1199–201.

[17] a) Liang G, Weng L, Lam JWY, Qin W, Tang BZ. Crystallization-induced hybrid nano-sheets of fluorescent polymers with aggregation-induced emission characteristics for sensitive explosive detection. ACS Macro Lett 2014;3:21–5;
b) Qian L, Tong B, Shen J, Shi J, Zhi J, Dong Y, et al. Crystallization-induced emission enhancement in a phosphorus-containing heterocyclic luminogen. J Phys Chem B 2009;113:9098–103;
c) Mazumdar P, Das D, Sahoo GP, Salgado-Morán G, Misra A. Aggregation induced emission enhancement from Bathophenanthroline microstructures and its potential use as sensor of mercury ions in water. Phys Chem Chem Phys 2014;16:6283–93.

[18] Dong YQ, Lam JWY, Qin AJ, Li Z, Sun JZ, Sung HHY, et al. Switching the light emission of (4-biphenylyl)phenyldibenzofulvene by morphological modulation: crystallization-induced emission enhancement. Chem Commun 2007: 40–2.

[19] a) Bu L, Li Y, Wang J, Sun M, Zheng M, Liu W, et al. Synthesis and piezochromic luminescence of aggregation-enhanced emission 9,10-bis(N-alkylcarbazol-2-yl-vinyl-2)anthracenes. Dyes Pigments 2013;99:833–8;
b) Sun M, Zhang D, Li Y, Wang J, Gao Y, Yang W. Aggregation-enhanced emission and piezochromic luminescence of 9,10-bis(p-dibutylaminostyryl)-2,6-bis(p-t-butylstyryl)anthracene. J Luminescence 2014;148:55–9;
c) Deng S, Hsiao T, Shih K, Hong J. Protein quantitation by complexation of fluorescent tetraphenylthiophene cation to anion-terminated poly(N-isopropylacrylamide): aggregation-enhanced emission and electrostatic interaction. J Photochem Photobiol B 2014;138:134–40;
d) Cao X, Zeng X, Mu L, Chen Y, Wang R, Zhang Y, et al. Characterization of the aggregation-induced enhanced emission, sensing, and logic gate behavior of 2-(1-hydroxy-2-naphthyl)methylene hydrazone. Sens Actuat B Chem 2013;177:493–9.

[20] a) Jintoku H, Ihara H. Molecular gel-mediated UV-to-visible spectral conversion for enhancement of power-conversion efficiency. Chem Commun 2012;48:1144–6;
b) Yoon S, Varghese S, Park SK, Wannemacher R, Gierschner J, Park SY. Color-tuned, highly emissive dicyanodistyrylbenzene single crystals: manipulating intermolecular stacking interactions for spontaneous and stimulated emission characteristics. Adv Opt Mater 2013;1:232–7;
c) Tiekink ERT, Zukerman-Schpector J. The importance of π-interactions in crystal engineering: frontiers in crystal engineering. Weinheim: Wiely-VCH Verlag GmbH; 2012.

[21] a) Xue P, Lu R, Chen G, Zhang Y, Nomoto H, Takafuji M, et al. Functional organogel based on a salicylideneaniline derivative with enhanced fluorescence emission and photochromism. Chem Eur J 2007;13:8231–9;
b) Chang C, Bhongale CJ, Lee C, Huang W, Hsu C, Diau EW. Relaxation dynamics and structural characterization of organic nanobelts with aggregation-induced emission. J Phys Chem C 2012;116:15146–54.

[22] Liu Y, Tao X, Wang F, Shi J, Sun J, Yu W, et al. Intermolecular hydrogen bonds induce highly emissive excimers: enhancement of solid-state luminescence. J Phys Chem C 2007;111:6544–9.

[23] a) Rajeswara M, Liao C, Sun S. Structurally simple thienodipyrandione-containing reversible fluorescent switching piezo- and acido-chromic materials. J Mater Chem C 2013;1:6386–94;
b) Kwon MS, Gierschner J, Seo J, Park SY. Rationally designed molecular D–A–D triad for piezochromic and acidochromic fluorescence on–off switching. J Mater Chem C 2014;2:2552–7.